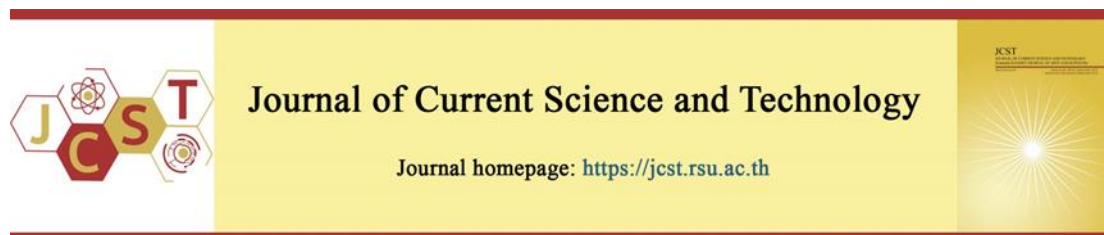


Cite this article: Kumar, A., Dahiya, S., Singh, N., & Singh, M. (2022, January). Brillouin amplification in compound (A^{III}B^V and A^{II}B^{VI}) semiconductors: effects of piezoelectricity, doping and external magnetostatic field. *Journal of Current Science and Technology*, 12(1), 61-78. DOI:



Brillouin amplification in compound (A^{III}B^V and A^{II}B^{VI}) semiconductors: effects of piezoelectricity, doping and external magnetostatic field

Arun Kumar¹, Sunita Dahiya¹, Navneet Singh², and Manjeet Singh^{3*}

¹Department of Physics, Baba Mastnath University, AsthalBohar – 124021 (Rohtak) India

²Department of Physics, Rajiv Gandhi Government College for Women, Bhiwani-127021, India

³Department of Physics, Government College, Matanhail – 124106 (Jhajjar) India

*Corresponding author; E-mail: msgur_18@yahoo.com

Received 1 July 2021; Revised 7 October 2021; Accepted 28 October 2021;

Published online 25 January 2022

Abstract

In this paper, a theoretical study describing stimulated Brillouin amplification in compound (A^{III}B^V and A^{II}B^{VI}) semiconductors is explored. The effects of piezoelectric coefficient, free carrier concentration, and applied magnetic field on the threshold intensity for exciting the stimulated Brillouin amplification and the parameters characterizing stimulated Brillouin amplification, viz. stimulated Brillouin amplification coefficient, transmitted intensity of first-order Brillouin scattered Stokes mode, and Brillouin cell efficiency of the Brillouin cell are estimated. Numerical analysis is made for three different Brillouin cells consisting of n-InSb, n-GaAs and n-CdS at 77K illuminated by a nanosecond pulsed CO₂ laser. Endeavors are coordinated towards determining the appropriate values of free carrier (doping) concentration and magnetostatic field to improve the parameters characterizing stimulated Brillouin amplification, at smaller excitation intensity, and to establish the suitability of Brillouin cells consisting of compound (A^{III}B^V and A^{II}B^{VI}) semiconductors as hosts for manufacture of Brillouin amplifiers and Brillouin oscillators.

Keywords: A^{III}B^V and A^{II}B^{VI} semiconductors; Brillouin cell efficiency; Laser-semiconductor interactions; stimulated Brillouin amplification.

1. Introduction

Stimulated Brillouin scattering (SBS) is a well-known four-wave mixing (FWM) nonlinear optical effect. It is notable for its significant applications in optical pulse compression, (spatial and temporal) optical signal processing, optical phase conjugation (OPC), etc. (Hon, 1982; Damzen, & Hutchinson, 1983; Guo, Lu, & Wang, 2010; Omatsu et al., 2012). Optical pulse compression (from nanoseconds to picoseconds) via SBS has been used to initiate internal confinement fusion (Perkins, Betti, La Fortune, & Williams, 2009; Schmitt, Bates, Obenschain,

Zalesak, & Fyfe, 2010). SBS based FWM nonlinear optical effect, known as Brillouin-enhanced FWM (BE-FWM), yields efficient optical phase conjugate signals (Scott, & Ridley, 1989; Singh, & Aghamkar, 2008; Bhan, Singh, Kumar, & Singh, 2019). SBS based optical phase conjugate mirrors (SBS-OPCMs) have been used in reimbursement of coherent electromagnetic waves distortions generated by optical elements of the laser systems and consequently improving their overall performance. This methodology permits use of the laser systems for wide range of applications needing distortion-free coherent electromagnetic waves

(Brignon, & Jean-Pierre, 2012). Stimulated Brillouin amplification based distributed optical fiber sensors (SBA-DOFSs) have been fabricated for their potential applications in higher resolution temperature sensing in engineering (Shimizu, Horiguchi, Koyamada, & Kurashima, 1993; Bao, & Chen, 2012).

Stimulated Brillouin amplification (SBA) is SBS based nonlinear optical process, where a coherent acoustical phonon mode generated via material's electrostriction and piezoelectricity properties under intense laser irradiation causes scattering of the coherent (pump) wave. Consequently, Stokes/anti-Stokes modes of various orders, with leftover energy equivalent to vibrational energy levels of the material's medium, are generated. Like other stimulated scattering processes, this process also caused the amplification of generated as well as scattered modes for pump fields over threshold. SBA is well known for its potential applications in diverse areas of modern optics (Smith, Atkins, Cotter, & Wyatt, 1986). It has been used in optical fiber communication systems, allowing in-line distributed signal amplification and all-band wavelength coverage (Terra, Grosche, & Schnatz, 2010; Sheng, Ba, & Lu, 2019).

Literature survey reveals that optical fibers have been widely employed as Brillouin media for SBA to study the optical parameters over a wide range of experiments (Williams, Bao, & Chen, 2014; Bai et al., 2018). The important parameters influencing the SBA in a Brillouin medium for a specific use are the amplification coefficient, the transmitted intensity, the transmitted wavelength, the optical damage threshold, size constraints, pumping conditions, etc. Even though different Brillouin media exhibit identical characteristics under different conditions but the parameters of a Brillouin medium under different conditions can vary extensively (You, Bongu, Bao, & Panoiu, 2019). Therefore, it becomes essential to choose a suitable Brillouin medium as per explicit necessity. The various designs of Brillouin amplification medium, depending on various Brillouin media adopted are advantageous. Thus, beside optical fibers, a Brillouin amplification medium may be a cell filled with a gas or liquid medium, a bulk crystal, or a waveguide in on-chip photonic circuits.

Giant SBA at low threshold has been demonstrated in all the four states of matter including solids (Kittlaus, Shin, & Rakich, 2016),

liquids (Wu, Khizhnyak, & Markov, 2010), gases (Yang, Gyger, & Thevenaz, 2020) and plasmas (Trines et al., 2020). Among the rich variety of Brillouin amplification media, bulk compound ($A^{III}B^V$ and $A^{II}B^{VI}$) semiconductor have proved their potential in photonic devices fabrication owing to their well-developed manufacturing technology, monitoring of carrier's life-time (via device structuring and designing), device functioning under either normal/oblique incidence or in waveguides, and integrating devices with other photonic devices. Additionally, these materials offer giant optical nonlinearities under off-resonant transitions; which may be enhanced further by externally applied-magnetic/electric fields (Mokkapati, & Jagadish, 2009; Sweeney, & Mukherjee, 2017). Thus, the choice of compound $A^{III}B^V$ and $A^{II}B^{VI}$ type semiconductors as Brillouin media for studying SBA is indubitable.

From an extensive literature survey (Salimullah, Sharma, & Tripathi, 1980; Gupta & Sen, 2001; Sharma, & Ghosh, 2002; Singh, Aghamkar, & Sen, 2007; Uzma, Zeba, Shah, & Salimullah, 2009; Gökhan, Göktaş, & Sorger, 2018), it appears that various theoretical formulations have been carried out to study SBS and to explore the possibility of SBA over threshold in piezoelectric $A^{III}B^V$ type semiconductors; but no theoretical/experimental research work has been done until now to study SBA in compound $A^{III}B^V$ and $A^{II}B^{VI}$ type semiconductors where the dependence of parameters characterizing SBA, viz. SBA coefficient, Brillouin cell efficiency, transmitted intensity of Brillouin-scattered Stokes mode (BSSM), etc. on free carrier concentration and applied magnetic field have been explored. Moreover, in the previously reported works, the phenomenon of SBS and possibility of SBA over threshold has been studied in piezoelectric $A^{III}B^V$ semiconductors by including the piezoelectric and electrostrictive coefficients phenomenologically; the role of these coefficients on nonlinearity of the Brillouin medium has not been explored. In compound $A^{III}B^V$ and $A^{II}B^{VI}$ type semiconductors, the coherent collective plasmon-cyclotron oscillations strongly coupled together via piezoelectricity (Ghosh, Sharma, Khare, & Salimullah, 2004). Moreover, piezoelectric property of the compound $A^{III}B^V$ and $A^{II}B^{VI}$ type semiconductors insights the essential propagation characteristics (Singh & Singh, 2021). Hence the role of piezoelectric property of the compound

$A^{III}B^V$ and $A^{II}B^{VI}$ type semiconductors in theoretical study of SBA over threshold is significant from the fundamental point of view.

In light of the richness of the possible impact of semiconductor material's piezoelectric property, free carrier (doping) concentration and applied magnetic field on Brillouin nonlinearity, in this paper, the authors presented a theoretical model to analyze their effect on the parameters characterizing SBA in compound $A^{III}B^V$ and $A^{II}B^{VI}$ type semiconductors. This study may be technically useful in the development of Brillouin amplifiers and Brillouin oscillators for their potential applications in optical signal processing and nonlinear spectroscopy. The compound $A^{III}B^V$ and $A^{II}B^{VI}$ type semiconductors selected as Brillouin media are assumed to be irradiated by an intense coherent (pump) wave under off-resonant transition regime, i.e. $\hbar\omega_0 \ll \hbar\omega_g$; where $\hbar\omega_g$ and $\hbar\omega_0$ are the semiconductor band-gap and pump wave energies, respectively. This condition allows the charge carriers (here electrons) of compound $A^{III}B^V$ and $A^{II}B^{VI}$ type semiconductors to significantly influence the Brillouin nonlinearity; neglecting the contributions of photo-induced inter-band transition mechanisms (Toudert, & Serna, 2017). The nonlinear mechanisms taken are: (i) the induced nonlinear polarization originating via material's electrostrictive property, and (ii) the induced nonlinear polarization originating via material's induced carrier density. An expression is obtained for the net value of Brillouin susceptibility. The threshold intensity for exciting SBA as well as the parameters characterizing SBA, i.e. the SBA coefficient, the transmitted intensity of BSSM and the Brillouin cell efficiency are estimated. Finally, numerical analysis is performed for three different Brillouin cells consisting of n-InSb, n-GaAs (as representative $A^{III}B^V$ type), and n-CdS (as representative $A^{II}B^{VI}$ type) semiconductors, at 77K temperature and illuminated by a pulsed CO₂ laser at 10.6 μm wavelength.

2. Objectives

The objectives of the present analytical investigation is to study the influence of semiconductor material's piezoelectric property, free carrier concentration, and applied magnetic field on threshold characteristics for exciting SBA and the parameters (viz. SBA coefficient, transmitted intensity of BSSM, and Brillouin cell

efficiency) characterizing SBA of compound $A^{III}B^V$ and $A^{II}B^{VI}$ type semiconductors/laser (viz. n-InSb/CO₂ laser, n-GaAs/ CO₂ laser, and n-CdS CO₂ laser) systems. Efforts are made to find out the appropriate values of free carrier concentration and applied magnetic field to enhance the parameters characterizing SBA, at lower excitation intensity, and to establish the suitability of compound $A^{III}B^V$ and $A^{II}B^{VI}$ type semiconductors as potential candidate materials for development of efficient Brillouin amplifiers and Brillouin oscillators.

3. Theoretical formulations

In order to study the effects of material's piezoelectric property, free carrier concentration, and applied magnetic field on SBA in compound $A^{III}B^V$ and $A^{II}B^{VI}$ type semiconductors, we consider the fluid model of semiconductor-plasmas (Chefranov, & Chefranov, 2020). The phenomenon of SBS arises as a result of nonlinear coupling among three coherent fields, viz. an acoustical phonon mode, an intense electromagnetic (pump) field, and a scattered first-order Stokes component of pump field represented by $u(x, t) = u_0 \exp[i(k_a x - \omega_a t)]$, $E_0(x, t) = E_0 \exp[i(k_0 x - \omega_0 t)]$, and $E_s(x, t) = E_s \exp[i(k_s x - \omega_s t)]$, respectively. These fields are connected to each other via momentum and energy conservation relations: $\hbar\vec{k}_0 = \hbar\vec{k}_a + \hbar\vec{k}_s$ and $\hbar\omega_0 = \hbar\omega_a + \hbar\omega_s$, respectively. The compound $A^{III}B^V$ and $A^{II}B^{VI}$ type semiconductors (chosen as Brillouin media) are subjected to an applied magnetic field represented as: $\vec{B}_0 = \hat{z}B_0$.

In doped $A^{III}B^V$ and $A^{II}B^{VI}$ type semiconductors, under coherent pump irradiation, the lattice vibrations (at induced acoustical phonon mode frequency ω_a) generate electron density fluctuations (at electron-plasma frequency ω_p). Under the influence of applied magnetic field, the induced acoustical phonon mode couples nonlinearly with pump field derives electron-plasma wave at difference and sum frequencies. For pump fields well above the threshold, the scattered first-order Stokes component of pump field as well as induced acoustical phonon mode gets amplified under phase matching constraints.

In the chosen Brillouin media, let x be the lattice position and $u(x, t)$ be the departure of atoms from its lattice position (along x-axis) in order that

the strain produced is given by $\frac{\partial u(x,t)}{\partial x}$. Following Singh and Singh (2021), one may express the equation of motion of $u(x, t)$ as:

$$\rho \frac{\partial^2 u(x,t)}{\partial t^2} - C \frac{\partial^2 u(x,t)}{\partial x^2} + 2\rho\Gamma_a \frac{\partial u(x,t)}{\partial t} = F_e(\beta, \gamma), \quad (1a)$$

Where ρ represents the mass density of Brillouin medium. C stands for the elastic coefficient in order that the acoustical phonon mode velocity in the Brillouin medium may be expressed as: $v_a = (C/\rho)^{1/2}$. To consider the damping of acoustical phonon mode, the term $2\rho\Gamma_a \frac{\partial u(x,t)}{\partial t}$ is considered phenomenologically. $F_e(\beta, \gamma)$ stands for the net force generated in unit volume accomplished by the chosen Brillouin media in the presence pump electromagnetic field given by (Singh & Singh, 2021).

$$F_e(\beta, \gamma) = F_\beta^{(1)} + F_\gamma^{(2)}, \text{ in which}$$

$$\rho \frac{\partial^2 u(x,t)}{\partial t^2} - C \frac{\partial^2 u(x,t)}{\partial x^2} + 2\rho\Gamma_a \frac{\partial u(x,t)}{\partial t} = -\beta \frac{\partial E_1}{\partial x} + \frac{\gamma}{2} \frac{\partial}{\partial x} (E_0 E_1^*). \quad (1b)$$

Other equations used in present theoretical formulation are:

$$\frac{\partial \vec{v}_0}{\partial t} + v\vec{v}_0 + \left(\vec{v}_0 \cdot \frac{\partial}{\partial x} \right) \vec{v}_0 = -\frac{e}{m} (\vec{E}_e) = -\frac{e}{m} [\vec{E}_0 + (\vec{v}_0 \times \vec{B}_0)] \quad (2)$$

$$\frac{\partial \vec{v}_1}{\partial t} + v\vec{v}_1 + \left(\vec{v}_0 \cdot \frac{\partial}{\partial x} \right) \vec{v}_1 + \left(\vec{v}_1 \cdot \frac{\partial}{\partial x} \right) \vec{v}_0 = -\frac{e}{m} [\vec{E}_1 + (\vec{v}_0 \times \vec{B}_0)] \quad (3)$$

$$\frac{\partial n_1}{\partial t} + n_0 \frac{\partial v_1}{\partial x} + n_1 \frac{\partial v_0}{\partial x} + v_0 \frac{\partial n_1}{\partial x} = 0 \quad (4)$$

$$\vec{P}_{es} = -\gamma \frac{\partial u}{\partial x} (\vec{E}_0) \quad (5)$$

$$\frac{\partial E_1}{\partial x} + \frac{\beta}{\epsilon} \frac{\partial^2 u}{\partial x^2} + \frac{\gamma}{\epsilon} \frac{\partial^2 u}{\partial x^2} (E_0) = -\frac{n_1 e}{\epsilon}. \quad (6)$$

Eqs. (2) – (6) and the notations used are well explained in Ref. (Singh & Singh, 2021; Singh, Aghamkar, Kishore, & Sen, 2008).

The forces $F_\beta^{(1)}$ and $F_\gamma^{(2)}$ generate carrier (here electrons) concentration perturbations in the chosen Brillouin media. These density perturbations have been obtained by the procedure

$F_\beta^{(1)} = -\beta \frac{\partial E_1}{\partial x}$ represents the first-order force arising due to piezoelectric property, and

$F_\gamma^{(2)} = \frac{\gamma}{2} \frac{\partial}{\partial x} (E_0 E_1^*)$ stands for second-order force arising due to electrostrictive property of medium.

Here the parameters γ and β stand for the electrostriction and piezoelectric constants of the chosen Brillouin media, respectively. E_1 is space charge electric field. Under high frequency pump electromagnetic wave irradiation, the ions of the chosen Brillouin Media Shift to non-symmetrical sites, generally bringing about a contraction in the pump field direction and an expansion in a direction perpendicular to it. The electrostrictive property has its origin in the electrostrictive force thus produced in the Brillouin media. The coupling of elastic stiffness constant of the Brillouin media with high frequency pump electromagnetic field generates the piezoelectric force in the Brillouin media.

Substituting the value of $F_e(\beta, \gamma)$ in Eq. (1a)), the equation for $u(x, t)$ becomes

adopted by Singh & Singh (2021). We differentiate Eq. (4), substitute the partial differentials of v_0 and v_1 from Eqs. (2) and (3), respectively, E_1 from Eq. (6), and after mathematical simplification, obtain the coupled equation of carrier density perturbations as:

$$\frac{\partial^2 n_1}{\partial t^2} + v \frac{\partial n_1}{\partial t} + \bar{\omega}_p^2 n_1 + \frac{n_0 e k_s^2 u^*}{m \epsilon_1} (\beta \gamma \delta_1 \delta_2 A + \gamma^2 E_0^2) E_0 E_s^* = i n_1 k_s \bar{E}, \quad (7)$$

where $\bar{E} = \frac{e}{m} (\bar{E}_e)$, $A = \frac{\omega_p^2}{(e/m)k_a}$, $\delta_1 = 1 - \frac{\omega_c^2}{(\omega_0^2 - \omega_c^2)}$, $\delta_2 = 1 - \frac{\omega_c^2}{(\omega_s^2 - \omega_c^2)}$,

$\bar{\omega}_{pc} = v \left(\frac{\omega_p \omega_c}{\omega_p^2 + \omega_c^2} \right)$ (coupled plasmon-cyclotron frequency),

$\omega_c = \frac{e}{m} B_0$ (electron-cyclotron frequency), and

$\omega_p = \left(\frac{n_0 e^2}{m \epsilon} \right)^{1/2}$ (electron-plasma frequency).

We may express the perturbed electron concentration n_1 as: $n_1 = n_{1f}(\omega_s) + n_{1s}(\omega_a)$, where n_{1s} (known as low-frequency component) oscillates at coherent induced acoustical mode frequency ω_a while n_{1f} (known as high-frequency component) is associated with coherent electromagnetic waves at frequencies $\omega_0 \pm q\omega_a$, where Q is an integer. The coherent electromagnetic fields at difference (i.e. $\omega_0 - q\omega_a$) and sum (i.e. $\omega_0 + q\omega_a$) frequencies are designated as Stokes and anti-Stokes modes, respectively. It is well known that in SBS processes, the anti-Stokes modes are very weak and hence they can be neglected in comparison to the Stokes modes. For the chosen Brillouin media, when either laser-semiconductor interaction length or pump intensity varies ($\geq 10^{12}$ Wm⁻²), then rate of energy flow from coherent pump electromagnetic field to first-order Stokes mode (i.e. $\omega_s = \omega_0 - \omega_a$) becomes much large and consequently the intensity of first-order Stokes mode approaches to that of pump wave, subsequently causing the depletion of pump wave. At long last, the first-order Stokes mode serves as

an energy source for higher-order Stokes modes (i.e. $\omega_0 - 2\omega_a$, $\omega_0 - 3\omega_a$, $\omega_0 - 4\omega_a$, ...etc) amplification (Wolff, Stiller, Eggleton, Steel, & Poulton, 2017). The intensity of higher-order Stokes modes is also pump pulse dependent. For example, for a pump wave of pulse duration ~0.35 nanoseconds and intensity $\sim 3.2 \times 10^{12}$ Wcm⁻² interacts with InSb crystal of interaction length ~ 30 cm; the intensities of transmitted wave, first-order Stokes modes, and second-order Stokes mode are nearly equal (30% each) while the intensity of third- and fourth-order Stokes modes diminished by 10^4 and 10^{12} times, respectively (Velchev, & Ubachs, 2001). These outcomes demonstrate that for the chosen Brillouin media of sample length ~ few centimeter at pump intensity $\sim 10^{12}$ Wm⁻² with pulse duration $\sim 10^{-9}$ s, the lower-order Stokes modes are nearly equally intense, while the higher-order Stokes components are too less intense to be neglected. In the present analytical investigation, the study of SBA in compound A^{III}B^V and A^{II}B^{VI} type semiconductors of millimeter dimensions confined at moderate pump intensity with pulse duration much larger than induced coherent acoustical phonon life time, i.e. under steady-state operation. Under such conditions, the emission of higher-order Stokes modes can be neglected and the emission first-order Stokes mode which is responsible for occurrence of SBA needs to be considered (Singh & Singh, 2021).

Eq. (7), under rotating-wave approximation (RWA), leads to following coupled equations:

$$\frac{\partial^2 n_{1f}}{\partial t^2} + v \frac{\partial n_{1f}}{\partial t} + \bar{\omega}_{pc}^2 n_{1f} + \frac{n_0 e k_s^2 u^*}{m \epsilon_1} (\beta \gamma \delta_1 \delta_2 A + \gamma^2 E_0^2) E_0 E_s^* = -i n_{1s}^* k_s \bar{E} \quad (8a)$$

and

$$\frac{\partial^2 n_{1s}}{\partial t^2} + v \frac{\partial n_{1s}}{\partial t} + \bar{\omega}_{pc}^2 n_{1s} = i n_{1f}^* k_s \bar{E}. \quad (8b)$$

Eqs. (8a, b) reveal that the pump electromagnetic field (\bar{E}) is responsible for the coupling of fast and slow components (n_{1f} , n_{1s}) of electron density perturbations.

Solving the coupled wave Eqs. (8a, b) and using Eq. (1b), we obtained an expression for n_{1s} as:

$$n_{1s} = \frac{n_0 k_a k_s (\beta \gamma \delta_1 \delta_2 A + \gamma^2 E_0^2) E_0 E_s^*}{2\rho \epsilon \delta_3 (\omega_0^2 - \omega_c^2 + 2iv\omega_0)(\omega_a^2 - k_a^2 v_a^2 + 2i\Gamma_a \omega_a)}, \quad (9)$$

where $\Omega_{ps}^2 = \bar{\omega}_{pc}^2 - \omega_s^2$, and $\Omega_{pa}^2 = \bar{\omega}_{pc}^2 - \omega_a^2$ and $\delta_3 = 1 - \frac{(\Omega_{ps}^2 - iv\omega_s)(\Omega_{pa}^2 + iv\omega_a)}{k_s^2 \bar{E}^2}$.

The components of oscillatory electron fluid velocity, under coherent pump electromagnetic wave irradiation and presence of an applied magnetic fields, may be obtained from Eq. (2) as:

$$v_{0x} = \frac{e}{m(v - i\omega_0)} E_0, \quad (10a)$$

and

$$v_{0y} = \frac{e[\omega_c + (v - i\omega_0)]}{m[\omega_c^2 + (v - i\omega_0)^2]} E_0. \quad (10b)$$

The perturbed current density (at first-order Stokes mode frequency ω_s) is obtained via perturbed carrier concentration as (Singh & Singh, 2021):

$$J_{cd}(\omega_s) = n_{1s}^* e v_{0x} = \frac{k_a k_s \omega_p^2 (v - i\omega_0) (\beta \gamma \delta_1 \delta_2 A + \gamma^2 E_0^2) |E_0|^2 E_s^*}{2\rho \delta_3 (\omega_0^2 - \omega_c^2 + 2iv\omega_0)(\omega_a^2 - k_a^2 v_a^2 + 2i\Gamma_a \omega_a)} \quad (11)$$

The nonlinear induced polarization (at first-order Stokes mode frequency ω_s) is obtained via perturbed current density as (Singh & Singh, 2021):

$$P_{cd}(\omega_s) = \frac{-J_{cd}(\omega_s)}{i\omega_s} = \frac{k_a k_s \omega_p^2 \omega_0^3 (\beta \gamma \delta_1 \delta_2 A + \gamma^2 E_0^2) |E_0|^2 E_s^*}{2\rho \omega_s \delta_3 (\omega_0^2 - \omega_c^2 + 2iv\omega_0)(\omega_a^2 - k_a^2 v_a^2 + 2i\Gamma_a \omega_a)} \quad (12)$$

Defining the induced polarization (at first-order Stokes mode frequency ω_s) as:

$$P_{cd}(\omega_s) = \epsilon_0 (\chi_B^{(3)})_{cd} |\bar{E}_0|^2 E_s^*, \text{ the Brillouin susceptibility } (\chi_B^{(3)})_{cd} \text{ is given by}$$

$$(\chi_B^{(3)})_{cd} = \frac{k_a k_s \omega_p^2 \omega_0^3 [\beta \gamma \delta_1 \delta_2 A + (2\gamma^2 / \eta c \epsilon_0) I_0]}{2\rho \epsilon_0 \omega_s \delta_3 (\omega_0^2 - \omega_c^2 + 2iv\omega_0)(\omega_a^2 - k_a^2 v_a^2 + 2i\Gamma_a \omega_a)} \quad (13)$$

where $I_0 = \frac{1}{2} \eta c \epsilon_0 |E_0|^2$ is the intensity of pump wave (Singh & Singh, 2021).

In addition to $P_{cd}(\omega_s)$, the chosen Brillouin media also exhibit material's electrostriction property based polarization $P_{es}(\omega_s)$

originating via nonlinear interaction between the coherent pump electromagnetic wave and the induced acoustical phonon mode. Following Ref. (Singh & Singh, 2021) and using Eqs. (1) and (5), we obtain

$$P_{es}(\omega_s) = \frac{k_a k_s \omega_0^4 \gamma^2}{2\rho(\omega_0^2 - \omega_c^2 + 2iv\omega_0)(\omega_a^2 - k_a^2 v_a^2 + 2i\Gamma_a \omega_a)} |E_0|^2 E_s^* \quad (14)$$

As a result, the corresponding Brillouin susceptibility $(\chi_B^{(3)})_{es}$ is given by

$$(\chi_B^{(3)})_{es} = \frac{k_a k_s \omega_0^4 \gamma^2}{2\rho \epsilon_0 (\omega_0^2 - \omega_c^2 + 2iv\omega_0)(\omega_a^2 - k_a^2 v_a^2 + 2i\Gamma_a \omega_a)} \quad (15)$$

Using Eqs. (13) and (15), the effective Brillouin susceptibility is given by

$$(\chi_B^{(3)})_e = (\chi_B^{(3)})_{es} + (\chi_B^{(3)})_{cd} = \frac{k_a k_s \omega_0^4 \gamma^2}{2\rho \epsilon_0 (\omega_0^2 - \omega_c^2 + 2iv\omega_0)(\omega_a^2 - k_a^2 v_a^2 + 2i\Gamma_a \omega_a)} \left(1 + \frac{\delta_4 \delta_5}{\delta_3} \right), \quad (16)$$

where $\delta_4 = 1 + (\beta/\gamma)\delta_1\delta_2A$ and $\delta_5 = \frac{2I_0\omega_p^2}{\eta c\epsilon_0\omega_0\omega_s}$.

A look at Eq. (16) reveals that $(\chi_R^{(3)})_e$ is complex. It may be written as: $(\chi_B^{(3)})_e = [(\chi_B^{(3)})_e]_r + i[(\chi_B^{(3)})_e]_i$, where $[(\chi_B^{(3)})_e]_r$ represent the real part while $[(\chi_B^{(3)})_e]_i$ stands for the imaginary part of complex $(\chi_B^{(3)})_e$. Rationalization of Eq. (16) yield

$$[(\chi_B^{(3)})_e]_r = \frac{k_a k_s \omega_0^4 \gamma^2 (\omega_a^2 - k_a^2 v_a^2)(\omega_0^2 - \omega_c^2)}{2\rho\epsilon_0[(\omega_0^2 - \omega_c^2)^2 + 4v^2\omega_0^2][(\omega_a^2 - k_a^2 v_a^2)^2 + 4\Gamma_a^2\omega_a^2]} \left(1 + \frac{\delta_4\delta_5}{\delta_3}\right) \quad (17a)$$

and

$$[(\chi_B^{(3)})_e]_i = -\frac{2k_a k_s v\omega_0^5 \omega_a \Gamma_a \gamma^2}{\rho\epsilon_0[(\omega_0^2 - \omega_c^2)^2 + 4v^2\omega_0^2][(\omega_a^2 - k_a^2 v_a^2)^2 + 4\Gamma_a^2\omega_a^2]} \left(1 + \frac{\delta_4\delta_5}{\delta_3}\right). \quad (17b)$$

The threshold pump intensity for exciting SBA may be obtained via condition: $[(\chi_B^{(3)})_e]_i = 0$. This yields

$$I_{0,th} = \frac{\eta\epsilon_0 c \omega_0 \omega_s \delta_3}{2\omega_p^2 \delta_4}. \quad (18)$$

For $I_0 > I_{0,th}$, the SBA coefficient g_B may be obtained via relation (Boyd, 2008):

$$g_B = -\frac{k_s}{4\eta^3 \epsilon_0 c} [(\chi_B^{(3)})_e]_i I_0 = \frac{k_a k_s^2 v \omega_0^5 \omega_a \Gamma_a \gamma^2 I_0}{2\rho\epsilon_0^2 \eta^3 c [(\omega_0^2 - \omega_c^2)^2 + 4v^2\omega_0^2][(\omega_a^2 - k_a^2 v_a^2)^2 + 4\Gamma_a^2\omega_a^2]} \left(1 + \frac{\delta_4\delta_5}{\delta_3}\right). \quad (19)$$

The transmitted amplitude of BSSM E_T may be obtained via relation (Simoda, 1982):

$$E_T = \frac{-iLk_s [(\chi_B^{(3)})_e]_i}{\epsilon_1} |E_0|^2 E_s^*.$$

Using Eq. (16), the transmitted intensity of BSSM (assuming $L \geq 10^2 \lambda_0$; λ_0 being the pump wavelength) is given by

$$I_T = \frac{1}{2} \eta c \epsilon_0 |E_T|^2 = \frac{8k_a^2 k_s^4 v^2 \omega_0^{10} \omega_a^2 \Gamma_a^2 \gamma^4 L^2 I_0^2}{\epsilon \epsilon_1 \eta c \rho^2 [(\omega_0^2 - \omega_c^2)^2 + 4v^2\omega_0^2]^2 [(\omega_a^2 - k_a^2 v_a^2)^2 + 4\Gamma_a^2\omega_a^2]^2} \left(1 + \frac{\delta_4\delta_5}{\delta_3}\right)^2 |E_s|^2. \quad (20)$$

The Brillouin cell efficiency is given by

$$\eta_B = \frac{I_T}{I_0} = \frac{8k_a^2 k_s^4 v^2 \omega_0^{10} \omega_a^2 \Gamma_a^2 \gamma^4 L^2 I_0}{\epsilon \epsilon_1 \eta c \rho^2 [(\omega_0^2 - \omega_c^2)^2 + 4v^2\omega_0^2]^2 [(\omega_a^2 - k_a^2 v_a^2)^2 + 4\Gamma_a^2\omega_a^2]^2} \left(1 + \frac{\delta_4\delta_5}{\delta_3}\right)^2 |E_s|^2. \quad (21)$$

Eqs. (18) - (21) show that $I_{0,th}$, g_B , I_T and η_B are influenced by β and γ (via parameter δ_4), n_0 (via ω_p and hence δ_3), and B_0 (via ω_c , δ_1 , δ_2 , δ_3 and δ_4). $I_{0,th}$ and g_B are independent while I_T and η_B are dependent of Brillouin cell length L .

4. Results and discussion

The threshold intensity ($I_{0,th}$) for exciting SBA and the parameters (g_B , I_T and η_B) characterizing SBA in the presence of applied magnetic field (i.e. $B_0 \neq 0$) and finiteness of piezoelectric coefficient ($\beta \neq 0$) can be studied

from Eqs. (18) – (21). On the other hand, in the absence of either/both applied magnetic field and piezoelectricity, the parameters characterizing SBA can be obtained by following substitutions:

- (i) In the absence of an applied magnetic field (i.e. $B_0 = 0$): $\omega_c = 0$, $\delta_1 = 0$, $\delta_2 = 0$, hence $\delta_3 = 0$ and $\delta_4 = 0$.

(ii) In the absence of piezoelectricity (i.e. $\beta = 0$): $\delta_4 = 0$.

With these substitutions, it comes out that the parameters characterizing SBA for cases: (a) absence of applied magnetic field (i.e. $B_0 = 0$) and presence of piezoelectricity (i.e. $\beta \neq 0$), and (b) absence of both applied magnetic field (i.e. $B_0 = 0$) and piezoelectricity (i.e. $\beta = 0$) are identical. Thus it may be concluded that the piezoelectric property of the chosen Brillouin media contribute to SBA only in the appearance of applied magnetic field. In addition, finiteness of the electrostriction coefficient

($\gamma \neq 0$) is pre-requisite condition for SBA to occur. The parameters characterizing SBA become independent of free carrier concentration (n_0) when either/both applied magnetic field and material's piezoelectric property are absent (i.e. $B_0 = 0$ or $\beta = 0$).

For numerical analysis, we consider the irradiation of three different Brillouin cells consisting of n-InSb, n-GaAs and n-CdS by $10.6 \mu\text{m}$ ($\omega_0 = 1.78 \times 10^{14} \text{ s}^{-1}$) CO₂ laser at 77 K. The material parameters of the representative samples are given in Table 1 (Singh & Singh, 2021; Adachi, 1985).

Table 1 Material parameters of InSb, GaAs, and CdS

Parameter	InSb	GaAs	CdS
Density, ρ (kg m ⁻³)	5.8×10^3	5.3×10^3	4.82×10^3
Electron's effective mass, m	$0.014m_0$	$0.063m_0$	$0.107m_0$
Acoustic wave velocity, v_a (ms ⁻¹)	4×10^3	4.7×10^3	1.8×10^3
Dielectric constant, ϵ_1	15.8	12.9	9.35
Piezoelectric coefficient, β (Cm ⁻²)	0.054	0.16	0.21
Electrostrictive coefficient, γ (Fm ⁻¹)	3×10^{11}	1×10^{11}	7.6×10^{10}
Electron collision frequency, ν (s ⁻¹)	3.5×10^{11}	4×10^{11}	4×10^{13}

For the chosen Brillouin cells, at liquid nitrogen (77K) temperature,

- (i) the coefficient of absorption is quite low and the contributions arising due to inter-band transitions may be safely neglected (Toudert & Serna, 2017);
- (ii) the dominating process for the carrier's energy and momentum transfer to the first-order Stokes mode is because of acoustic phonon mode scattering around $10 \mu\text{m}$ (Gahlawat, Singh, & Dahiya, 2021).

Using the same model as presented here, hot carrier effects on real and imaginary parts of Brillouin susceptibilities of n-InSb/CO₂ laser system (Kumari & Sharma, 2021), parametric amplification characteristics of n-InSb/CO₂ laser and n-CdS/CO₂ laser systems (Singh & Singh, 2021), and modulational amplification characteristics of n-GaAs/CO₂ laser system (Dubey, Paliwal, & Ghosh, 2019) have been recently studied by assuming the generation of acoustical phonon

mode in the semiconductor medium at 77K temperature.

Eqs. (19) – (21) contain some common terms which significantly influence the parameters characterizing SBA. These terms can be explained as follows:

- (i) In term $1 + (\delta_4 \delta_5 / \delta_3)$, the parameter δ_5 is intensity dependent. For the material parameters of different Brillouin cells given in Table 1, at pump intensities $I_0 < I_c$ ($5.15 \times 10^{13} \text{ Wm}^{-2}$ for n-InSb, $4.72 \times 10^{13} \text{ Wm}^{-2}$ for n-GaAs, and $3.97 \times 10^{13} \text{ Wm}^{-2}$ for n-CdS), $(\delta_4 \delta_5 / \delta_3) < 1$; the parameter $\delta_4 \delta_5 / \delta_3$ can be neglected in comparison to unity and the parameters characterizing SBA become dependent on electrostrictive coefficient only. However, at pump intensities $I_0 > I_c$, $(\delta_4 \delta_5 / \delta_3) > 1$; the parameter $\delta_4 \delta_5 / \delta_3$ plays important role in

the analysis and the parameters characterizing SBA depends on β as well as γ (via parameter δ_4).

- (ii) The term $(\omega_a^2 - k_a^2 v_a^2)^2$ occurs due to dispersion characteristics of the acoustical phonon mode. At particular values of k_a , for which $\omega_a \approx k_a v_a$, the term $(\omega_a^2 - k_a^2 v_a^2)^2 \rightarrow 0$ yielding enhanced values of parameters characterizing SBA for a fixed pump intensity.
- (iii) The term $(\omega_0^2 - \omega_c^2)^2$ becomes important when magneto static field dependent electron-cyclotron frequency becomes comparable to pump wave frequency. For $\omega_c^2 \approx \omega_0^2$, the term $(\omega_0^2 - \omega_c^2)^2 \rightarrow 0$ yielding enhanced parameters characterizing SBA for a fixed pump intensity.
- (iv) The parameter Ω_{ps}^2 (in term δ_3), by increasing B_0 continuously in the considered range and decreasing n_0 proportionally, allows to resonate coupled

plasmon-cyclotron mode at Stokes shifted frequency, i.e. $\bar{\omega}_{pc}^2 \sim \omega_s^2$.

- (v) The parameter Ω_{pa}^2 (in term δ_3), allows to resonate coupled plasmon-cyclotron mode frequency at acoustical mode frequency, i.e. $\bar{\omega}_{pc}^2 \sim \omega_a^2$; but for the considered range of B_0 , extremely high values of n_0 are required. The high values of free carrier concentration will lead to diffusion effects and the theoretical formulation developed here becomes questionable.

Using Eqs. (18) – (21), the dependence of threshold pump intensity ($I_{0,th}$) for exciting SBA on applied magnetic field (B_0) and free carrier concentration (n_0) and the dependence of parameters (g_B , I_T and η_B) characterizing SBA on applied magnetic field (B_0), free carrier concentration (n_0), pump intensity (I_0), and Brillouin cell length (L) for three different Brillouin cells consisting on n-InSb, n-GaAs, and n-CdS is explored in detail. The results are plotted in Figures. 1 – 6.

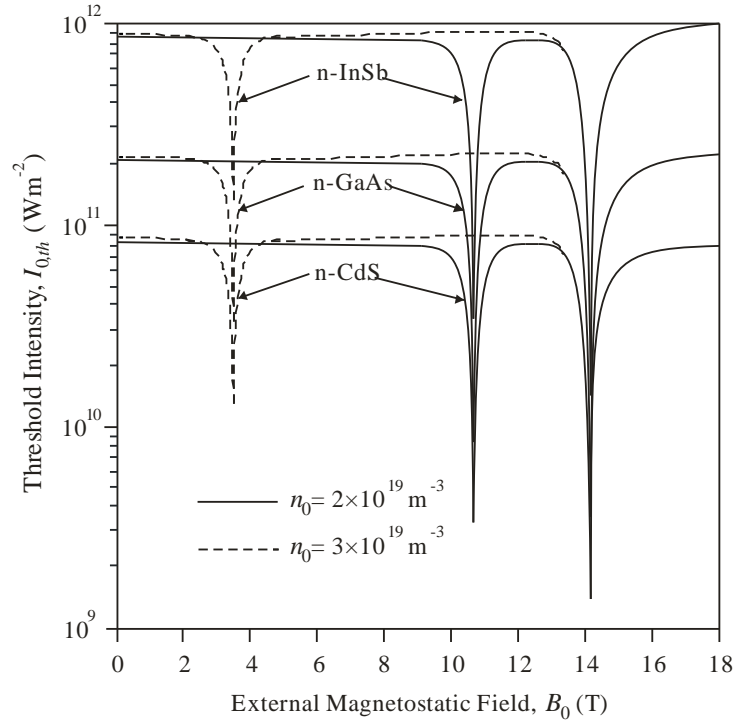


Figure 1 Variation of $I_{0,th}$ with B_0 at two different values of n_0

Figure 1 depicts variation of the threshold intensity ($I_{0,th}$) for exciting SBA with applied magnetic field (B_0) for two different free carrier concentrations ($n_0 = 2 \times 10^{19} \text{ m}^{-3}$ and $3 \times 10^{19} \text{ m}^{-3}$). We observed that for a given free carrier concentration, the threshold intensity is relatively larger and remain constant with respect to applied magnetic field in regime $0 < B_0 < 9.5 \text{ T}$ for $n_0 = 2 \times 10^{19} \text{ m}^{-3}$ and $0 < B_0 < 2.7 \text{ T}$ for $n_0 = 3 \times 10^{19} \text{ m}^{-3}$. With further rising applied magnetic field beyond this value, the threshold intensity starts decreasing, attaining its minimum at $B_0 = 10.5 \text{ T}$ at $n_0 = 2 \times 10^{19} \text{ m}^{-3}$ and $B_0 = 3.7 \text{ T}$ for $n_0 = 3 \times 10^{19} \text{ m}^{-3}$. Increasing applied magnetic field further beyond these values causes the sharp rise of threshold intensity, achieving its older (higher) value $B_0 = 11.5 \text{ T}$ $n_0 = 2 \times 10^{19} \text{ m}^{-3}$ and $B_0 = 4.7 \text{ T}$ for and $n_0 = 3 \times 10^{19} \text{ m}^{-3}$ and thereafter remains

independent of applied magnetic field for $B_0 = 13 \text{ T}$. This segregate nature of threshold intensity arises due to resonance between coupled plasmon-cyclotron mode frequency ($\bar{\omega}_{pc}$) and scattered first-order Stokes mode frequency (ω_s), i.e. $\bar{\omega}_{pc}^2 \sim \omega_s^2$. At $B_0 = 13.5 \text{ T}$, the threshold intensity corresponding to the different free carrier concentrations, become exactly equal and thereafter display indistinguishable feature irrespective of free carrier concentration. At $B_0 = 14.2 \text{ T}$, the threshold intensity attains a minimum, irrespective of free carrier concentration. This minimum arises due to resonance between electron-cyclotron frequency (ω_c) and pump wave frequency (ω_0), i.e. $\omega_c^2 \sim \omega_0^2$. Thus the resonance conditions $\bar{\omega}_{pc}^2 \sim \omega_s^2$ and $\omega_c^2 \sim \omega_0^2$ lowers the threshold intensity for exciting SBA by one and two orders of magnitude, respectively.

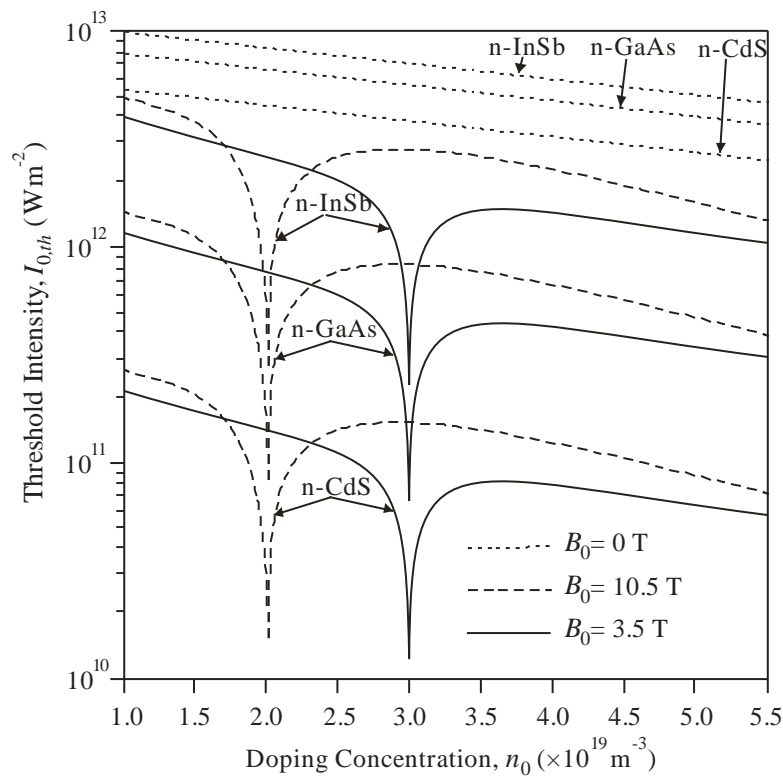


Figure 2 Variation of $I_{0,th}$ with n_0 for the cases: (i) $B_0 = 0 \text{ T}$ and (ii) $B_0 = 3.5, 10.5 \text{ T}$

Figure 2 displays variation of the threshold intensity ($I_{0,th}$) for exciting SBA with free carrier concentration (n_0) for the cases: (i) disappearance of applied magnetic field ($B_0 = 0$ T) and (ii) appearance of applied magnetic field ($B_0 = 3.5, 10.5$ T). It may be observed that the presence of increasing applied magnetic field is suitable for decreasing the threshold intensity for exciting SBA. The threshold intensity starts at a considerably higher value, decreases linearly throughout the plotted regime of free carrier concentration, except at $n_0 = 2 \times 10^{19} \text{ m}^{-3}$ (for $B_0 = 10.5$ T) and $n_0 = 3 \times 10^{19} \text{ m}^{-3}$ (for $B_0 = 3.5$ T). For these combinations of n_0 and B_0 , $I_{0,th}$ falls sharply. This behaviour occurs due to resonance condition: $\bar{\omega}_{pc}^2 \sim \omega_s^2$. On the other hand, in the disappearance of applied magnetic field, the threshold intensity is

relatively larger and decreases linearly with rising free carrier concentration of the chosen Brillouin cell. One may infer from this figure that around resonance, the threshold intensity for exciting SBA lowers by one order of magnitude than around off-resonance.

From Figures 1 and 2, it can be clearly seen that all the three different Brillouin cells consisting of n-InSb, n-GaAs and n-CdS exhibit similar threshold characteristics; the difference being that the SBA in n-CdS occurs at lowest threshold while in n-InSb occurs at highest threshold, i.e. $(I_{0,th})_{n\text{-CdS}} < (I_{0,th})_{n\text{-GaAs}} < (I_{0,th})_{n\text{-InSb}}$, throughout the plotted regimes of free carrier concentration and external magnetic field of the chosen Brillouin cells. The calculated values of threshold intensity for exciting SBA of n-InSb, n-GaAs and n-CdS are represented in Table 2.

Table 2 Calculated values of threshold intensity for exciting SBA for n-InSb, n-GaAs and n-CdS

Parameter	n_0 (m^{-3})	B_0 (T)	n-InSb	n-GaAs	n-CdS
Threshold pump intensity, $I_{0,th}$ (Wm^{-2})	2×10^{19}	0	8.5×10^{12}	6.8×10^{12}	4.5×10^{12}
	3×10^{19}	0	7.1×10^{12}	5.8×10^{12}	3.9×10^{12}
	2×10^{19}	10.5	3.0×10^{11}	8.9×10^{10}	1.6×10^{10}
	3×10^{19}	3.5	2.2×10^{11}	6.7×10^{10}	1.3×10^{10}

Figure. 3 shows variation of the parameters (g_B, I_T and η_B) characterizing SBA with applied magnetic field (B_0) for two different free carrier concentrations ($n_0 = 2 \times 10^{19} \text{ m}^{-3}$ and $3 \times 10^{19} \text{ m}^{-3}$) at excitation intensity $I_0 = 10^{12} \text{ Wm}^{-2}$ and Brillouin cell length $L = 0.5$ mm. We observed that for a given free carrier concentration, all these

three parameters display identical nature of curves with respect to applied magnetic field. This may be interpreted on the basis of resonances; as already explained in Figure 1; only the difference is that here, the curves showing the variation of parameters characterizing SBA with applied magnetic field shoots up rather shoots down as in case of variation of threshold intensity with applied magnetic field.

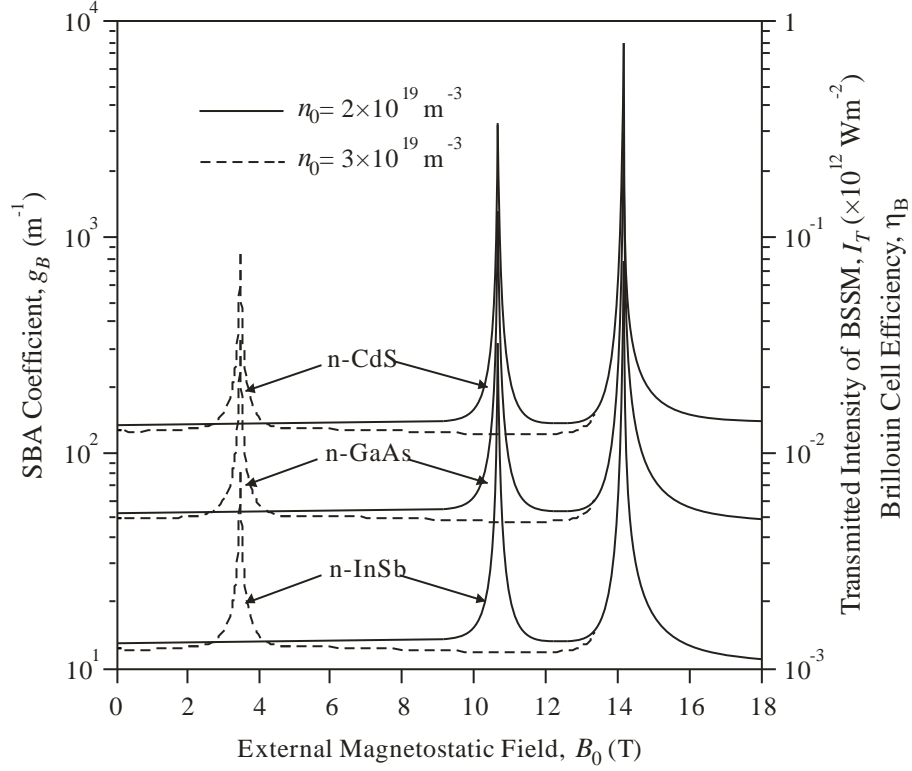


Figure 3 Variation of parameters (g_B , I_T and η_B) characterizing SBA with B_0 for two different values of n_0 at $I_0 = 10^{12} \text{ Wm}^{-2}$ and $L = 0.5 \text{ mm}$.

The interesting feature of resonance condition $\bar{\omega}_{pc}^2 \sim \omega_s^2$ is coupling between the electron-cyclotron mode (at frequency ω_c) and the electro-plasmon mode (at frequency ω_p). The resulting mode is known as coupled cyclotron-plasmon mode and it oscillates at frequency $\bar{\omega}_{pc}$. When this resulting mode interacts with the coherent pump electromagnetic field, coupled cyclotron-plasmon mode frequency dependent coherent scattered Stokes mode (at frequency ω_s) is emitted. It is beneficial to move ω_s to the favourable spectral regime by varying either/both free carrier concentration (n_0) and applied magnetic field (B_0). By continuously increasing n_0 (via ω_p and hence $\bar{\omega}_{pc}^2$) and decreasing B_0 (via ω_c and hence $\bar{\omega}_{pc}^2$) in the same proportion maintains $\bar{\omega}_{pc}^2 \sim \omega_s^2$ at fixed value of ω_s . If n_0 is increased and B_0 is decreased continuously in an arbitrary manner, without maintaining their proportion, ω_s shifts to other value. Here, by continuously

increasing n_0 from $2 \times 10^{19} \text{ m}^{-3}$ to $3 \times 10^{19} \text{ m}^{-3}$ and decreasing B_0 from 10.5T to 3.7T maintains the resonance condition $\bar{\omega}_{pc}^2 \sim \omega_s^2$ at a fixed value of ω_s . Ultimately, at $n_0 = 3.3 \times 10^{19} \text{ m}^{-3}$, the resonance occurs around $B_0 = 0 \text{ T}$ for a fixed value of ω_s . For $n_0 > 3.3 \times 10^{19} \text{ m}^{-3}$, the resonance condition shifts the value of ω_s .

The resonance condition $\omega_c^2 \sim \omega_0^2$, being independent of n_0 , occurs at fixed $B_0 = 14.2 \text{ T}$. Thus around resonances, the parameters (g_B , I_T and η_B) characterizing SBA increases sharply. In the chosen Brillouin media, the drift velocity of electrons, which is smaller than acoustical phonon mode velocity at off-resonances, becomes much larger than the acoustical phonon mode velocity around resonances. As a result of this, the rate of energy transfer from coherent pump electromagnetic field to acoustical phonon mode increases to a large extent and it leads to amplification of acoustical phonon mode and hence

scattered first-order Stokes mode thereby enhancing the parameters characterizing SBA.

An important consequence of the present analysis is the enhancement of the parameters characterizing SBA around resonances by varying independently/simultaneously the free carrier concentration and applied magnetic field in three

different Brillouin cells consisting of n-InSb, n-GaAs and n-CdS under off-resonant laser irradiation. The outcomes allow one to tune the scattered first-order Stokes mode over wide infrared spectral regime and reveal a strong possibility of development of SBA based frequency converters as well as widely tunable Brillouin oscillators.

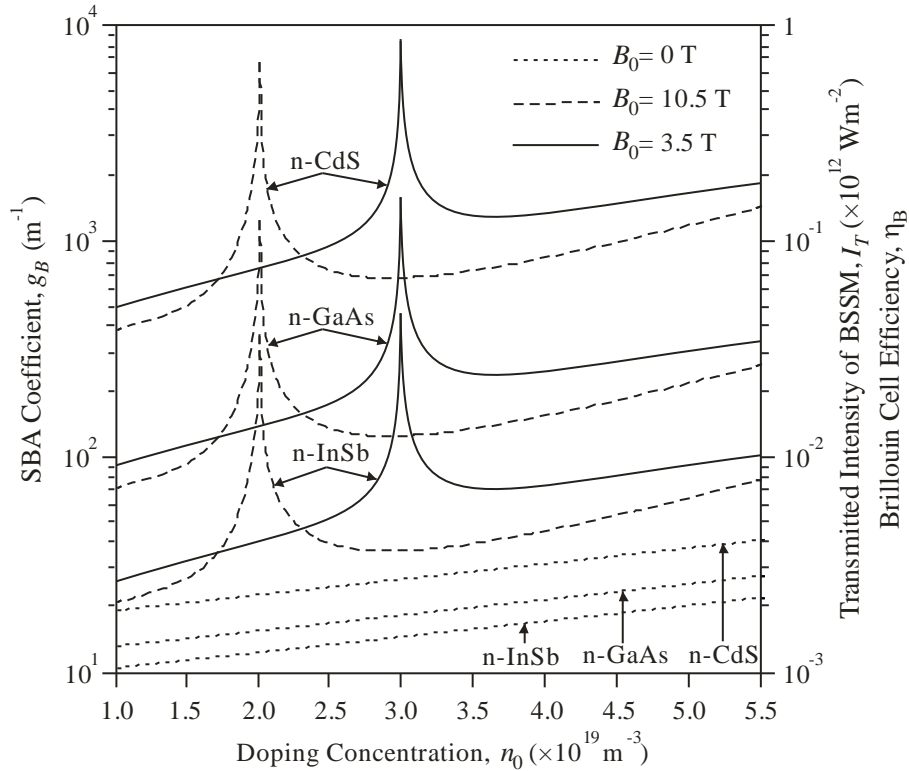


Figure 4 Variation of parameters (g_B , I_T and η_B) characterizing SBA with n_0 for the cases: (i) $B_0 = 0$ T and (ii) $B_0 = 3.5, 10.5$ T at $I_0 = 10^{12}$ Wm $^{-2}$ and $L = 0.5$ mm.

In Figure 4, the parameters (g_B , I_T and η_B) characterizing SBA are plotted versus free carrier concentration (n_0) for the cases: (i) disappearance of applied magnetic field ($B_0 = 0$ T) and (ii) appearance of applied magnetic field ($B_0 = 3.5, 10.5$ T) at excitation intensity $I_0 = 10^{12}$ Wm $^{-2}$ and Brillouin cell length $L = 0.5$ mm. It may be observed that the presence of increasing applied magnetic field is suitable for increasing the parameters characterizing SBA. These parameters start at a considerably lower value, increase linearly throughout the plotted regime of free carrier concentration, except at $n_0 = 2 \times 10^{19}$ m $^{-3}$ (for

$B_0 = 10.5$ T) and $n_0 = 3 \times 10^{19}$ m $^{-3}$ (for $B_0 = 3.5$ T). For these combinations of n_0 and B_0 , the parameters characterizing SBA increase sharply. This behaviour occurs due to resonance condition: $\bar{\omega}_{pc}^2 \sim \omega_s^2$. On the other hand, in the disappearance of applied magnetic field, the parameters characterizing SBA are relatively smaller and increase linearly with rising free carrier concentration of the chosen Brillouin cells. One may infer from this figure that around resonance, the parameters characterizing SBA enhance by one order of magnitude than around off-resonance.

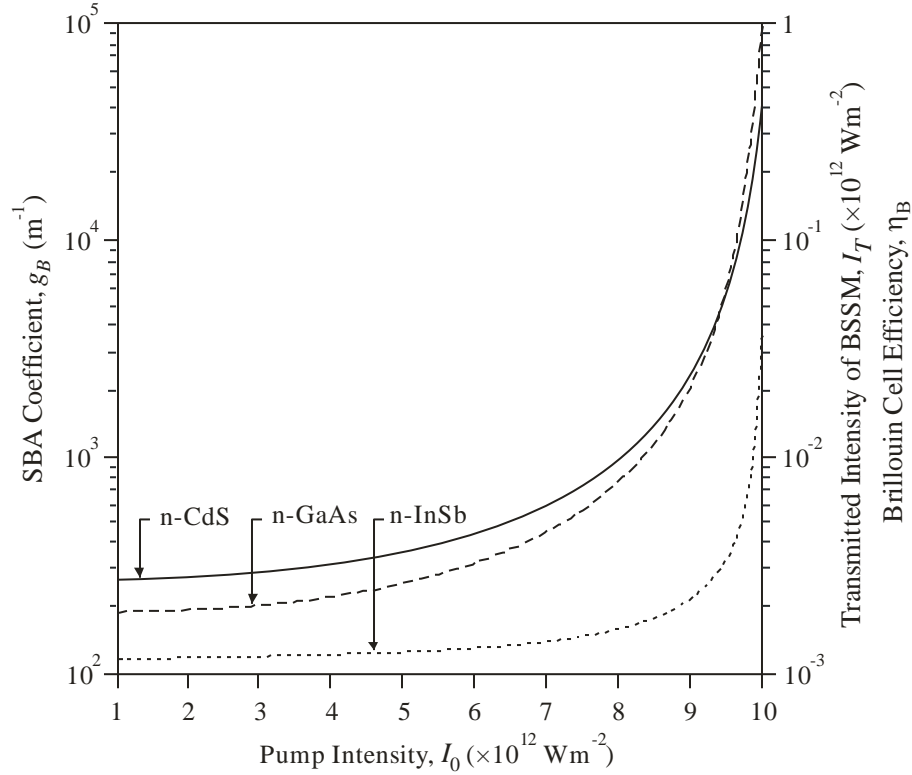


Figure 5 Variation of parameters (g_B , I_T and η_B) characterizing SBA with pump intensity (I_0) at $n_0 = 2 \times 10^{19} \text{ m}^{-3}$, $B_0 = 3.5 \text{ T}$ and $L = 0.5 \text{ mm}$.

Figure 5 depicts the nature of dependence of the parameters (g_B , I_T and η_B) characterizing SBA on pump intensity (I_0) at free carrier concentration $n_0 = 2 \times 10^{19} \text{ m}^{-3}$, applied magnetic field $B_0 = 3.5 \text{ T}$ and Brillouin cell length $L = 0.5 \text{ mm}$. It is found that the parameters characterizing SBA are relatively smaller and increase gradually with rise in pump intensity for $I_0 \leq 7 \times 10^{12} \text{ Wm}^{-2}$. Beyond this value of pump intensity, these parameters increase parabolically. Hence, higher power (pump) lasers are favourable to achieve larger value of the parameters characterizing SBA.

Practically, a highly intense pump beam may cause optical damage of the chosen Brillouin media. After performing a number of experiments on infrared laser-semiconductor interaction, Meyer, Bartoli, and Kruer (1980) concluded that when a semiconductor is exposed to a highly intense laser beam, a repeated consequence is the production of heat energy. For example, a Q-switched 170 nanoseconds pulsed CO_2 laser with pump intensity $\sim 10^{11} \text{ Wm}^{-2}$ causes an optical damage of InSb crystal

room temperature (Kruer, Esterowitz, Bartoli, & Allea, 1977). The mechanisms such as free carrier nonlinear absorption and use of ultra-short pulsed lasers have been suggested to increase the optical damage threshold intensity of $\text{A}^{\text{III}}\text{B}^{\text{V}}$ and $\text{A}^{\text{II}}\text{B}^{\text{VI}}$ type semiconductors (Boggess, Smirl, Moss, Boyd, & Stryland, 1985). In the present analysis, the pump intensity of the infrared nanoseconds pulsed CO_2 laser is taken above the threshold intensity for exciting SBA but well below the optical damage threshold intensity of the chosen Brillouin media.

In Figure 6, the parameters (I_T and η_B) characterizing SBA are plotted versus Brillouin cell length L at excitation intensity $I_0 = 10^{12} \text{ Wm}^{-2}$, free carrier concentration $n_0 = 2 \times 10^{19} \text{ m}^{-3}$ and applied magnetic field $B_0 = 3.5 \text{ T}$. It may be observed that both the parameters exhibit identical nature of curves; $I_T, \eta_B \propto L^2$, as suggested by Eqs. (20) and (21). Both I_T and η_B increase in a parabolic manner with L . Hence, a Brillouin cell of longer dimensions is favourable to achieve larger value of Brillouin cell efficiency.

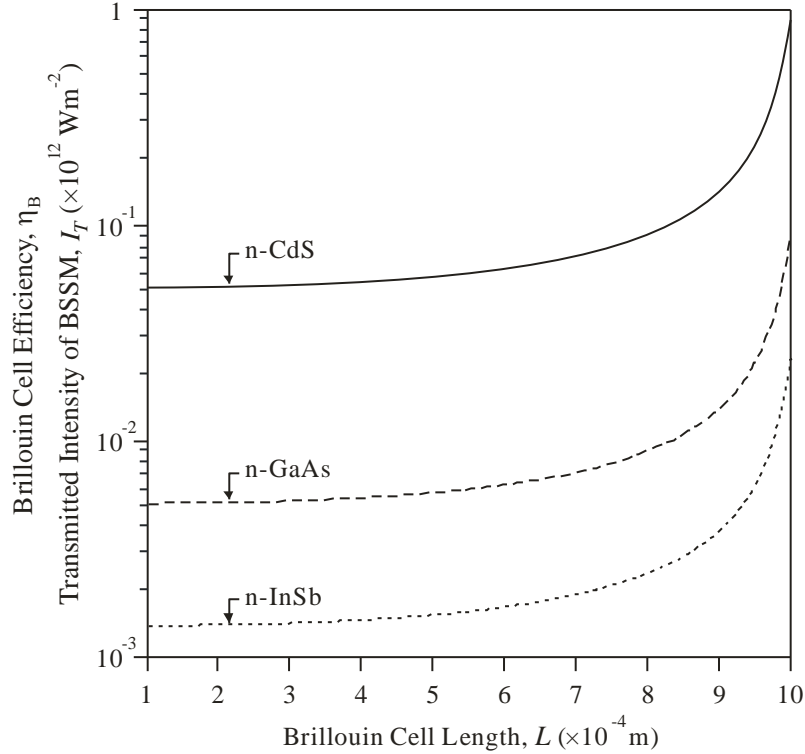


Figure 6 of parameters (I_T and η_B) characterizing SBA with Brillouin cell length L at $I_0 = 10^{12} \text{ Wm}^{-2}$, $n_0 = 2 \times 10^{19} \text{ m}^{-3}$ and $B_0 = 3.5 \text{ T}$

From Figures. 3 – 6, it is clearly understood that all the three different Brillouin cells consisting of n-InSb, n-GaAs and n-CdS exhibit similar SBA characteristics, the difference being that the parameters characterizing SBA are higher for a Brillouin cell having larger piezoelectric coefficient and smaller electrostriction coefficient,

i.e. $(g_B, I_T, \eta_B)_{n\text{-CdS}} > (g_B, I_T, \eta_B)_{n\text{-GaAs}} > (g_B, I_T, \eta_B)_{n\text{-InSb}}$, throughout the plotted regimes of free carrier concentration and applied magnetic field. Table 3 represents the calculated values of parameters characterizing SBA for three different Brillouin cells consisting of n-InSb, n-GaAs and n-CdS at $I_0 = 10^{12} \text{ Wm}^{-2}$ and $L = 0.5 \text{ mm}$.

Table 3 Calculated values of parameters characterizing SBA for three different Brillouin cells consisting of n-InSb, n-GaAs and n-CdS at $I_0 = 10^{12} \text{ Wm}^{-2}$ and $L = 0.5 \text{ mm}$.

Parameter	$n_0 \text{ (m}^{-3}\text{)}$	$B_0 \text{ (T)}$	n-InSb	n-GaAs	n-CdS
Brillouin gain coefficient, $g_B \text{ (m}^{-1}\text{)}$	2×10^{19}	0	12	15	23
	3×10^{19}	0	16	19	27
Transmitted intensity of BSSM, $I_T \text{ (Wm}^{-2}\text{)}$	2×10^{19}	10.5	3.7×10^2	1.3×10^3	7.8×10^3
	3×10^{19}	3.5	4.8×10^2	1.7×10^3	8.5×10^3
	2×10^{19}	0	1.2×10^9	1.5×10^9	2.3×10^9
Brillouin cell efficiency, η_B	3×10^{19}	0	1.6×10^9	1.9×10^9	2.7×10^9
	2×10^{19}	10.5	3.7×10^{10}	1.3×10^{11}	8.5×10^{11}
	3×10^{19}	3.5	4.8×10^{10}	1.7×10^{11}	8.5×10^{11}
Brillouin cell efficiency, η_B	2×10^{19}	0	1.2×10^{-3}	1.5×10^{-3}	2.3×10^{-3}
	3×10^{19}	0	1.6×10^{-3}	1.9×10^{-3}	2.7×10^{-3}
	2×10^{19}	10.5	0.037	0.13	0.78
	3×10^{19}	3.5	0.048	0.17	0.85

5. Conclusions

This paper deals with a theoretical study of SBA in compound ($A^{III}B^V$ and $A^{II}B^{VI}$) semiconductors. The influence of piezoelectricity, free carrier concentration, and external magnetostatic field on threshold characteristics for exciting SBA and the parameters (viz. SBA coefficient, transmitted intensity of BSSM, and Brillouin cell efficiency) characterizing SBA have been studied for three different semiconductors/laser (viz. n-InSb/CO₂ laser, n-GaAs/CO₂ laser, and n-CdS/CO₂ laser) systems. The study leads to following important conclusions:

1. The analysis offers two achievable resonance conditions ($\bar{\omega}_{pc}^2 \sim \omega_s^2, \omega_c^2 \sim \omega_0^2$) at which significant lowering in threshold intensity for exciting SBA and enhancement of parameters characterizing SBA can be obtained.
2. The parameters characterizing SBA increase with increasing pump intensity. The SBA coefficient is independent of Brillouin cell length but the transmitted intensity of BSSM and Brillouin cell efficiency increase with Brillouin cell length.
3. The comparison of threshold intensity and parameters characterizing SBA made for three different Brillouin cells consisting of n-InSb, n-GaAs and n-CdS reveals that the threshold intensity and parameters characterizing SBA exhibit exactly similar behaviour with respect to controllable parameters; the difference being that the threshold intensity (parameters characterizing SBA) is (are) smallest (largest) for n-CdS and largest (smallest) for n-InSb.
4. The study establishes the suitability of compound $A^{III}B^V$ and $A^{II}B^{VI}$ type semiconductors as potential candidate materials for development of efficient Brillouin amplifiers.

7. Acknowledgements

One of us (M. Singh) is highly thankful to Prof. Ashish Agarwal, Department of Physics, Guru Jambheshwar University of Science and Technology, Hisar for fruitful discussion and Prof. Sudhir Kumar, Department of English and Foreign Languages, M.D. University, Rohtak.

8. References

- Adachi, S. (1985). GaAs, AlAs, and Al_xGa_{1-x}As: Material parameters for use in research and device applications. *Journal of Applied Physics*, 58(3), R1-R29. DOI: 10.1063/1.336070
- Bai, Z., Yuan, H., Liu, Z., Xu, P., Gao, Q., Williams, R. J., ... & Lu, Z. (2018). Stimulated Brillouin scattering materials, experimental design and applications: A review. *Optical Materials*, 75, 626-645. DOI: 10.1016/j.optmat.2017.10.035
- Bao, X., & Chen, L. (2012). Recent progress in distributed fiber optic sensors. *sensors*, 12(7), 8601-8639. DOI: 10.3390/s120708601
- Bhan, S., Singh, H. P., Kumar, V., & Singh, M. (2019). Low threshold and high reflectivity of optical phase conjugate mode in transversely magnetized semiconductors. *Optik*, 184, 464-472. DOI: 10.1016/j.ijleo.2019.04.106
- Boggess, T., Smirl, A., Moss, S., Boyd, I., & Van Stryland, E. (1985). Optical limiting in GaAs. *IEEE journal of quantum electronics*, 21(5), 488-494. DOI: 10.1109/JQE.1985.1072688
- Boyd, R.W. (2008). *Nonlinear Optics*, Third Edition. New York, USA: Academic Press.
- Brignon, A., & Jean-Pierre, H. (2012). *Phase Conjugate Laser Optics*. New York, USA: John Wiley & Sons.
- Chefranov, S. G., & Chefranov, A. S. (2020). Hydrodynamic methods and exact solutions in applications to the electromagnetic field theory in medium. In: *Nonlinear Optics – Novel Results in Field Theory in Medium*. Lembrikov, B. (ed). Intechopen, UK.
- Damzen, M. J., & Hutchinson, M. H. R. (1983). High-efficiency laser-pulse compression by stimulated Brillouin scattering. *Optics letters*, 8(6), 313-315. DOI: 10.1364/OL.8.000313
- Dubey, S., Paliwal, A., & Ghosh, S. (2019). Transient amplification characteristics of frequency modulated wave in semiconductor plasmas. *Chinese Journal of Physics*, 61(5), 227-234. DOI: 10.1016/j.cjph.2019.08.010
- Gahlawat, J., Singh, M., & Dahiya, S. (2021). Piezoelectric and electrostrictive contributions to optical parametric amplification of acoustic phonons in

- magnetized doped III-V semiconductors. J. Optoelectron. *Journal of Optoelectronics and Advanced Materials*, 23(3-4), 183-192.
- Ghosh, S., Sharma, G. R., Khare, P., & Salimullah, M. (2004). Modified interactions of longitudinal phonon-plasmon in magnetized piezoelectric semiconductor plasmas. *Physica B: Condensed Matter*, 351(1-2), 163-170. DOI: 10.1016/j.physb.2004.06.001
- Gökhan, F. S., Göktaş, H., & Sorger, V. J. (2018). Analytical approach of Brillouin amplification over threshold. *Applied optics*, 57(4), 607-611. DOI: 10.1364/AO.57.000607
- Guo, Q., Lu, Z., & Wang, Y. (2010). Highly efficient Brillouin amplification of strong Stokes seed. *Applied Physics Letters*, 96(22), 221107. DOI: 10.1063/1.3435385
- Gupta, P. K., & Sen, P. K. (2001). Stimulated Brillouin scattering in n-type III-V piezoelectric semiconductors. *Journal of Nonlinear Optical Physics & Materials*, 10(2), 265-278. DOI: 10.1142/S0218863501000590
- Hon, D. T. (1982). Applications of wavefront reversal by stimulated Brillouin scattering. *Optical Engineering*, 21(2), 252-256. DOI: 10.1117/12.7972890
- Kittlaus, E. A., Shin, H., & Rakich, P. T. (2016). Large Brillouin amplification in silicon. *Nature Photonics*, 10(7), 463-467. DOI: 10.1038/nphoton.2016.112
- Kumari, P., & Sharma, B. S. (2021). Hot carrier effects on real and imaginary parts of Brillouin susceptibilities of semiconductor magneto-plasmas. *Journal of Current Science and Technology*, 11(3), 412-424.
- Kruer, M., Esterowitz, L., Bartoli, F., & Allea, R. (1977). The role of carrier diffusion in laser damage of semiconductor materials. In: *Laser Induced Damage in Optical Materials*, (eds.) Glass, A.J., & Guenther, A.H. NBS Special Publication No. 509, Washington, pp 473-480.
- Meyer, J. R., Bartoli, F. J., & Kruer, M. R. (1980). Optical heating in semiconductors. *Physical Review B*, 21(4), 1559. DOI: 10.1103/PhysRevB.21.1559
- Mokkapati, S., & Jagadish, C. (2009). III-V compound SC for optoelectronic devices. *Materials Today*, 12(4), 22-32. DOI: 10.1016/S1369-7021(09)70110-5
- Omatsu, T., Kong, H. J., Park, S., Cha, S., Yoshida, H., Tsubakimoto, K., ... & Gao, W. (2012). The current trends in SBS and phase conjugation. *Laser and Particle Beams*, 30(1), 117-174. DOI: 10.1017/S0263034611000644
- Perkins, L. J., Betti, R., LaFortune, K. N., & Williams, W. H. (2009). Shock ignition: A new approach to high gain inertial confinement fusion on the national ignition facility. *Physical review letters*, 103(4), 045004. DOI: 10.1103/PhysRevLett.103.045004
- Salimullah, M., Sharma, R. R., & Tripathi, V. K. (1980). Stimulated Brillouin scattering of laser radiation in a piezoelectric semiconductor in the presence of a magnetic field. *Journal of Physics D: Applied Physics*. 13(2), 117-125. DOI: 10.1088/0022-3727/13/2/008
- Schmitt, A. J., Bates, J. W., Obenschain, S. P., Zalesak, S. T., & Fyfe, D. E. (2010). Shock ignition target design for inertial fusion energy. *Physics of Plasmas*, 17(4), 042701. DOI: 10.1063/1.3385443
- Scott, A. M., & Ridley, K. D. (1989). A review of Brillouin-enhanced four-wave mixing. *IEEE journal of quantum electronics*, 25(3), 438-459. DOI: 10.1109/3.18560
- Sharma, G., & Ghosh, S. (2002). Stimulated Brillouin scattering in a magnetoactive III-V semiconductor: effects of carrier heating. *Physica B: Condensed Matter*, 322(1-2), 42-50. DOI: 10.1103/PhysRevB.47.16590
- Sheng, L., Ba, D., & Lu, Z. (2019). Imaging enhancement based on stimulated Brillouin amplification in optical fiber. *Optics express*, 27(8), 10974-10980. DOI: 10.1364/OE.27.010974
- Shimizu, K., Horiguchi, T., Koyamada, Y., & Kurashima, T. (1993). Coherent self-heterodyne detection of spontaneously Brillouin-scattered light waves in a single-mode fiber. *Optics letters*, 18(3), 185-187. DOI: 10.1364/OL.18.000185
- Simoda, K. (1982). Introduction to Laser Physics, Springer-Verlag, Berlin, pp. 160-166.

- Singh, M., & Aghamkar, P. (2008). Mechanism of phase conjugation via stimulated Brillouin scattering in narrow band gap semiconductors. *Optics communications*, 281(5), 1251-1255. DOI: 10.1016/j.optcom.2007.10.102
- Singh, M., Aghamkar, P., & Sen, P. K. (2007). Effect of doping on stimulated Brillouin scattering in piezoelectric magnetized III-V semiconductors. *Indian Journal of Pure and Applied Physics*, 45(6), 517-523.
- Singh, M., Aghamkar, P., Kishore, N., & Sen, P. K. (2008). Nonlinear absorption and refractive index of Brillouin scattered mode in piezoelectric semiconductor plasmas by an applied magnetic field. *Optics & Laser Technology*, 40(1), 215-222. DOI: 10.1016/j.optlastec.2007.02.001
- Singh, M., & Singh, M. (2021). Piezoelectric Contributions to Optical Parametric Amplification of Acoustical Phonons in Magnetized Doped III-V Semiconductors. *Iranian Journal of Science and Technology, Transactions A: Science*, 45(1), 373-382. DOI: 10.1007/s40995-020-00994-1
- Smith, D. W., Atkins, C. G., Cotter, D., & Wyatt, R. (1986). Application of Brillouin amplification in coherent optical transmission, *Proc. Opt. Fiber Commun. WE-3*, Atlanta Georgia, United States.
- Sweeney, S. J., & Mukherjee, J. (2017). Optoelectronic Devices and Materials. In: *Kasap, S. & Capper P. (eds) Springer Handbook of Electronic and Photonic Materials*. Springer Handbooks, Springer, Cham.
- Terra, O., Grosche, G., & Schnatz, H. (2010). Brillouin amplification in phase coherent transfer of optical frequencies over 480 km fiber. *Optics express*, 18(15), 16102-16111.
- Toudert, J., & Serna, R. (2017). Interband transitions in semi-metals, semiconductors, and topological insulators: a new driving force for plasmonics and nanophotonics. *Optical Materials Express*, 7(7), 2299-2325. DOI: 10.1364/OME.7.002299
- Trines, R. M. G. M., Alves, E. P., Webb, E., Vieira, J., Fiúza, F., Fonseca, R. A., ... & Bingham, R. (2020). New criteria for efficient Raman and Brillouin amplification of laser beams in plasma. *Scientific reports*, 10(1), 1-10. DOI: 10.1038/s41598-020-76801-z
- Uzma, C., Zeba, I., Shah, H. A., & Salimullah, M. (2009). Stimulated Brillouin scattering of laser radiation in a piezoelectric semiconductor: Quantum effect. *Journal of Applied Physics*, 105(1), 013307. DOI: 10.1063/1.3050340
- Velchev, I., & Ubachs, W. (2001). Higher-order stimulated Brillouin scattering with nondiffracting beams. *Optics letters*, 26(8), 530-532. DOI:10.1364/ol.26.000530
- Williams, D., Bao, X., & Chen, L. (2014). Characterization of high nonlinearity in Brillouin amplification in optical fibers with applications in fiber sensing and photonic logic. *Photonics Research*, 2(1), 1-9. DOI: 10.1364/PRJ.2.000001
- Wolff, C., Stiller, B., Eggleton, B. J., Steel, M. J., & Poulton, C. G. (2017). Cascaded forward Brillouin scattering to all Stokes orders. *New Journal of Physics*, 19(2), 023021.
- Wu, F. F., Khizhnyak, A., & Markov, V. (2010). A high Brillouin amplification using liquid fluorocarbon, *Proc. SPIE 7582, Nonlinear Frequency Generation and Conversion: Materials, Devices, and Applications IX*, 75821J.
- Yang, F., Gyger, F., & Thevenaz, L. (2020). Giant Brillouin amplification in gas using hollow-core waveguides. *Proc. CLEO*, Paper ID: SF2P.
- You, J. W., Bongu, S. R., Bao, Q., & Panoiu, N. C. (2019). Nonlinear optical properties and applications of 2D materials: theoretical and experimental aspects. *Nanophotonics*, 8(1), 63-97. DOI: 10.1515/nanoph-2018-0106